

4-10-2023

Evolution characteristics of meso-cracks in expansive soil under desiccating conditions

Hao-dong GAO

*School of Urban Construction, Wuhan University of Science and Technology, Wuhan, Hubei 430065, China,
State Key Laboratory of Geomechanics and Geotechnical Engineering, Institute of Rock and Soil
Mechanics, Chinese Academy of Sciences, Wuhan, Hubei 430071, China*

Ran AN

*School of Urban Construction, Wuhan University of Science and Technology, Wuhan, Hubei 430065, China,
State Key Laboratory of Geomechanics and Geotechnical Engineering, Institute of Rock and Soil
Mechanics, Chinese Academy of Sciences, Wuhan, Hubei 430071, China*

Follow this and additional works at: <https://rocksoilmech.researchcommons.org/journal>



Part of the [Geotechnical Engineering Commons](#)

Recommended Citation

GAO, Hao-dong and AN, Ran (2023) "Evolution characteristics of meso-cracks in expansive soil under desiccating conditions," *Rock and Soil Mechanics*: Vol. 44: Iss. 2, Article 7.

DOI: 10.16285/j.rsm.2022.5316

Available at: <https://rocksoilmech.researchcommons.org/journal/vol44/iss2/7>

This Article is brought to you for free and open access by Rock and Soil Mechanics. It has been accepted for inclusion in Rock and Soil Mechanics by an authorized editor of Rock and Soil Mechanics.

Evolution characteristics of meso-cracks in expansive soil under desiccating conditions

GAO Hao-dong^{1,2}, AN Ran^{1,2}, KONG Ling-wei², ZHANG Xian-wei², LEI Xue-wen¹

1. School of Urban Construction, Wuhan University of Science and Technology, Wuhan, Hubei 430065, China

2. State Key Laboratory of Geomechanics and Geotechnical Engineering, Institute of Rock and Soil Mechanics, Chinese Academy of Sciences, Wuhan, Hubei 430071, China

Abstract: Desiccation is the key factor causing the initiation and expansion of cracks in expansive soil. The evolution of cracks has a significant influence on the integrity of soil structure and the long-term stability and safety of the foundation. In order to investigate the evolution characteristics of dry-shrinkage cracks in expansive soil, micro-CT scanning tests were carried out on undisturbed soil samples. The 2D/3D images and characteristic parameters of soil mesocracks were obtained by using image processing technology, and the evolution of dry-shrinkage cracks was analyzed qualitatively and quantitatively. The results showed that the volumetric shrinkage characteristics of expansive soil in the drying process were restored by the 3D reconstructed digital model, which was in good agreement with the measured volume of samples. The quantitative indexes of mesocracks, such as crack ratio, crack number, crack volume, and crack structure characteristic parameters, can be extracted from micro-CT images. With the water content decreasing from 24.0% to 12.0%, the crack ratio and crack volume of expansive soil increased, while the number of cracks tended to decrease. Based on the volume and geometric characteristics of cracks, cracks can be divided into connected cracks and independent cracks. During the drying process, the volume proportion of connected cracks increased significantly, while the number of independent cracks decreased continuously. The 'ball-and-stick model' effectively simulated the geometric characteristics of the cracks in expansive soil. The equivalent pore radius, throat radius, throat length, and pore-throat coordination number all tended to increase during the drying process, and the connectivity of cracks was significantly enhanced. The SEM images showed that the connectivity of mesocracks was closely related to the arrangement of clay particles and the development of the pores between particles.

Keywords: expansive soil; desiccation; cracks; micro-CT test

1 Introduction

According to the latest assessment report of the United Nations Intergovernmental Panel on Climate Change (IPCC), global warming will continue to intensify in the coming decades^[1]. In the context of global warming, extreme arid climate-related disasters occur frequently in different regions. It can be predicted that the engineering geological problems and environmental problems caused by soil cracking induced by desiccation will become more and more serious. Expansive soil is a typical fractured soil, rich in strong hydrophilic minerals (mainly montmorillonite and illite). It has poor engineering characteristics such as strong hydrophilicity, crack development, easy shrinkage under dry conditions, and easy expansion when exposed to water^[2]. Expansive soil is widely distributed in the central provinces of China, Yunnan Province, Sichuan Province, Guizhou Province, etc., and it is one of the most common special soils in China's infrastructure construction^[3]. In the rainy season, hydrophilic clay minerals in expansive soil absorb water and swell, and the natural water content is close to saturation. However, in the arid and rain-less climate, the rapid evaporation of water leads

to a large area of cracking in expansive soil due to dry shrinkage, which has an extremely adverse effect on the engineering performance of the soil^[4–6]. Based on this, Kong et al.^[7], Yang et al.^[8], and Yao et al.^[9] all pointed out that if no necessary treatment measures are taken during project construction in areas where expansive soil is well distributed, the shrinkage deformation of expansive soil will result in serious engineering geological problems such as damage and cracking of a foundation, slope collapse, and deformation and destruction of subgrade and cutting.

Expansive soil can form complex network cracks under desiccating conditions. Accurate extraction and quantitative characterization of the morphology and size of cracks are critical prerequisites for clarifying the evolution mechanism of desiccation cracks^[10]. With the continuous development of detection techniques for the microstructure of geotechnical materials, research on the crack characteristics of expansive soil by using advanced measurement methods has received widespread attention. A large number of experimental studies have been carried out on the crack characteristics of expansive soil under desiccating conditions^[11–13]. Shi et al.^[14] observed the microscopic morphology of

Received: 16 March 2022

Accepted: 20 April 2022

This work was supported by the National Natural Science Foundation of China (12102312, 41372314) and the Open Research Fund of State Key Laboratory of Geomechanics and Geotechnical Engineering (SKLGME021018).

First author: GAO Hao-dong, male, born in 1999, Master candidate, focusing on soil mechanics of special soil. E-mail: Ghaohaodongf@wust.edu.cn

Corresponding author: AN Ran, male, born in 1992, Reader, research interests: environmental special soil engineering characteristics and geotechnical engineering. E-mail: anran@wust.edu.cn

cracks with environmental scanning electron microscopy (ESEM) and found that the formation process of desiccation cracks would cause irreversible structural damage to expansive soil. Tang et al.^[15–16] quantitatively analyzed the crack network of expansive soil using scanning electron microscopy (SEM) and digital image processing and discussed the evolution law of cracks in the process of desiccation, humidification, and wetting-drying cycle. They pointed out that matrix suction and tensile strength are the two key mechanical parameters that restrict the formation of cracks. Lu et al.^[17] conducted industrial CT scanning tests on Nanyang-remolded expansive soil and obtained the variation law of cracking degree with the increase of shrinkage volume based on two-dimensional image analysis. At present, although a large number of theoretical and experimental studies have been carried out on the volumetric shrinkage characteristics of expansive soil, due to the complexity and variability of cacks under desiccating conditions, the evolution law and the formation mechanism of mesocracks have not been deeply understood. Therefore, it is of great scientific significance to introduce advanced measuring methods for the quantitative analysis of cracks.

In light of the universality and harmfulness of desiccation cracks in expansive soil and the inadequacy of current studies, in this study, the undisturbed expansive soil samples are dried, and micro-CT scanning and three-dimensional reconstruction technology are used to extract and analyze the mesoscopic cracks in the process of desiccation. The rationality of using three-dimensional reconstruction model to analyze the evolution of cracks is discussed. Finally, the evolution law of desiccation cracks in expansive soil is expounded by calculating the quantitative parameters of mesoscopic cracks.

2 Materials and methods

2.1 Physical properties of materials

The expansive soil used in the test was taken from the slope of a foundation pit in Hefei City, Anhui Province, with a depth of 2–3 m below the ground surface. The basic physical properties and mineral composition of this expansive soil are listed in Table 1. In this study, the specific gravity G_s , natural water content w , maximum dry density ρ_{\max} , void ratio e , liquid limit w_L , plastic limit w_p , and free expansion rate δ_{ef} of the expansive soil were measured following the *Standard for geotechnical testing method* (GB/T 50123-2019)^[18]. The mineral composition of the expansive soil was determined by X-ray diffraction

(XRD) test, showing that this soil was mainly composed of hydrophilic clay minerals (44.1% montmorillonite) and non-clay minerals (32.2% quartz). The grading curve of the soil was measured by the sieve method and densitometer method, as shown in Figure 1. It can be seen that the expansive soil is mainly composed of clay particles (48% by weight) and silt particles (31% by weight).

2.2 Sample preparation and dehydration

According to the *Standard for geotechnical testing method* (GB/T 50123-2019)^[18], the undisturbed soil was trimmed into a standard cylindrical sample with a height of 80 mm and a diameter of 39.1 mm. Soil samples were dried in a constant temperature oven of which temperature was controlled at 40°C. When the water content of expansive soil approached the shrinkage limit, it did not change. The target water content in this test was expected to be controlled at 24.0%, 20.0%, 16.0%, and 12.0%. After drying the soil samples for different periods, the actual water content of expansive soil was obtained as 24.0%, 20.1%, 15.8%, and 12.0%, respectively.

2.3 Micro-CT scanning and analysis method

Micro-CT scanning technology uses X-ray sources to emit X-rays to penetrate the soil sample. Due to the different absorption capacities of materials with different densities to the same X-ray, the attenuation degree of X-ray intensity after penetrating the sample is different. Therefore, the composition of the material is detected by the change in light intensity before and after the X-ray passes through the sample, which is finally converted into high-resolution image information. The equation for calculating the attenuation degree of X-ray intensity of the material is as follows^[19]:

$$I = I_0 \exp(-\mu_m \chi \rho_t) \quad (1)$$

where I_0 and I are the intensities of X-ray before and after the X-ray penetrates the material; χ is the penetration length of incident X-ray; ρ_t is the density of the measured material; and μ_m is the absorption coefficient per unit mass^[20].

In a specific Micro-CT scanning environment, since μ_m and χ are only related to the wavelength and emission distance of incident rays, the attenuation degree of X-ray intensity is negatively correlated with the density of the material, and it is transformed into image information, showing that the materials with different densities show different gray levels in CT images^[21]. High-brightness areas represent the materials with high density, and low-brightness areas represent the materials with low density.

Table 1 Basic physical properties and mineral compositions of expansive soil

Specific gravity G_s	Water content w /%	Density ρ_{\max} /($\text{g} \cdot \text{cm}^{-3}$)	Void ratio e	Liquid limit w_L /%	Plastic limit w_p /%	Plastic index I_p	Free expansion rate δ_{ef} /%	Mineral compositions /%				
								Montmorillonite	Illite	Kaolinite	Quartz	Feldspar
2.7	24.5	1.74	0.72	72.5	32.6	39.9	97.3	44.1	4.7	5.5	32.2	13.5

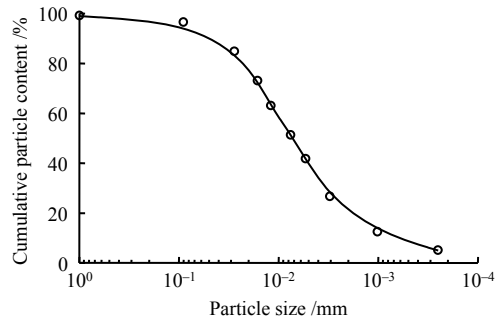


Fig. 1 Grain size distribution curve of expansive soil

The ZEISS XRadia 410 Micro-CT scanner with an accuracy of 0.1 μm was used to scan the internal structure of the expansive soil. The scanning system is mainly composed of an X-ray emission source, X-ray detector, scanning table, and computer system. The schematic diagram of the scanning process is shown in Fig.2. In the test, the soil sample was placed on the scanning table for 360° rotation. The X-ray was received by the detector after penetrating the sample. After calculation and analysis by the computer system, the high-resolution gray image was finally obtained.

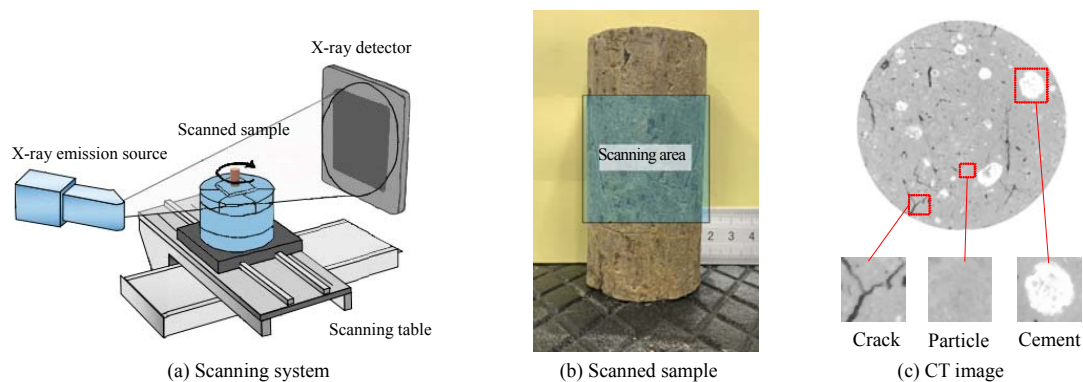


Fig. 2 Instruments, samples, and analysis process of micro-CT scanning tests

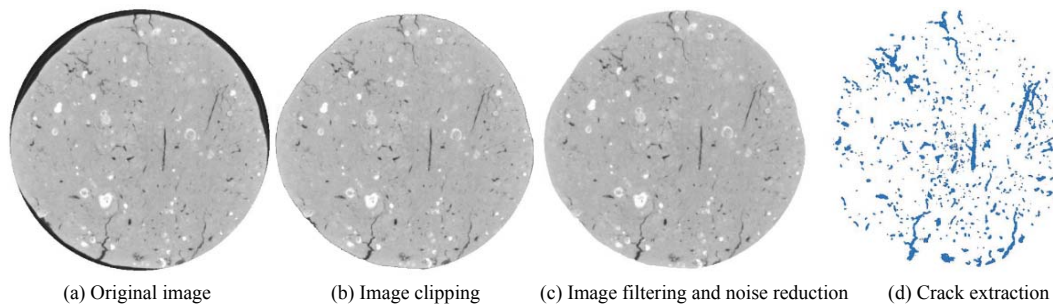


Fig. 3 CT image preprocessing process

3 Results and discussion

3.1 Volume variation of expansive soil during drying

Based on the results of micro-CT scanning, the number of pixels in the 3D digital model of expansive soil in the process of desiccation was counted, and then the total volume of the scanned area was calculated. According to the total number of pixels and volume calculation results, the volume of the scanned area at

The scanning height of the sample was about 30 mm, and the actual measured volume of the sample in the scanning area is 28.15 cm^3 . A total of 850 gray images with a spatial resolution of 35 μm were obtained. According to the gray image, the cracks, soil particles, and high-density cement inside the expansive soil can be divided into black, gray, and white areas, respectively.

Accurate extraction of soil cracks in micro-CT scanning images is the key to subsequent quantitative analysis. In this test, the 3D visualization software AVIZO was used to preprocess the original CT image to eliminate the effects of the defects of the sample itself and the noise in the scanning process on the crack extraction. The original image obtained by micro-CT scanning is shown in Fig.3(a). After removing the fixed base and the metal ring part, the trimmed two-dimensional image was obtained, as shown in Fig.3(b). Then the median filtering method was used for noise reduction, and the noise reduction image as shown in Fig.3(c) was obtained. Finally, according to the processed micro-CT scanning of a gray image, the Otsu algorithm was used to determine the segmentation gray threshold, and the mesocracks within the expansive soil were accurately extracted, as shown in Fig. 3(d).

the initial water content is 27.97 cm^3 , which was very close to the measured sample volume (28.15 cm^3), indicating that the micro-CT scanning results can accurately reflect the volumetric shrinkage characteristics of expansive soil during drying. Figure 4 shows the variation of the calculated volume of the scanned area of expansive soil with the decrease in water content. It can be seen that the volume of expansive soil presents a trend of gradual shrinkage in the process of desiccation,

and the change rate is first fast and then slow. During the whole desiccation process, the volume of the expansive soil sample decreased by 1.83 cm^3 , and the volumetric shrinkage rate was about 6.54%. During the process of water content decreasing from 20.1% to 15.8%, the volumetric shrinkage changed the most, about 3.04%, and the volume decreased by about 0.85 cm^3 , accounting for 46.45% of the total shrinkage.

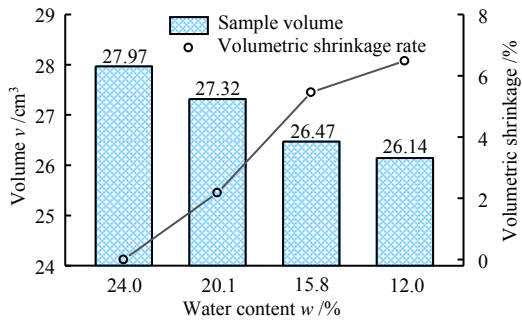


Fig. 4 Variation of sample volume at different water content

3.2 Two-dimensional cracks

The 450th CT scanning section was extracted for two-dimensional rendering, as shown in Fig.5. It can be seen that the number of original cracks inside the expansive soil was relatively small. When the water content decreased from 24.0% to 20.1%, the cracks in expansive soil increased slowly and the secondary cracks gradually emerged. At this time, the cracks were mainly locally isolated cracks, and the connectivity between the cracks was relatively low. As the water content decreased to 15.8%, the edge of the section showed obvious irregular depression and shrinkage, and there were many secondary cracks extending from the edge to the inside of the sample. When the water content decreased to 12.0%, the secondary cracks further propagated and coalesced, forming a complex two-dimensional crack network, and the volumetric shrinkage of the expanded soil sample further increased.

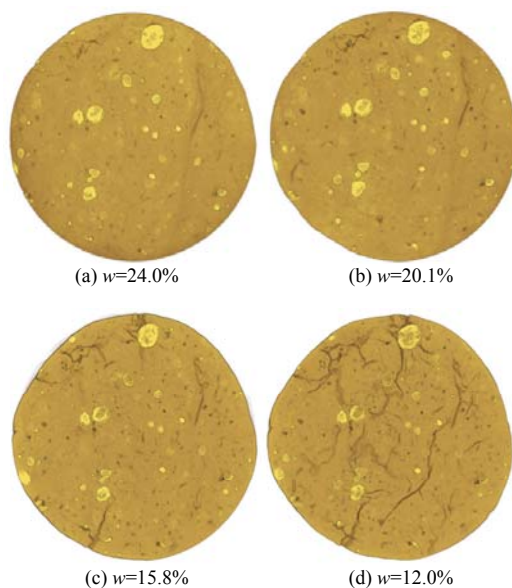


Fig. 5 2D CT scanning images of expansive soil

Crack ratio is one of the main parameters to characterize the physical properties of soil. Due to the inherent anisotropy of soil, the distribution characteristics of cracks along the axial direction of the sample are different and uneven distribution of crack ratio could be found. By calculating the ratio of the pixel area of the crack to the total pixel area of the soil sample in the micro-CT scanning image, the surface crack ratio S_i and the average surface crack ratio \bar{S} of the four groups of soil samples with different water contents were calculated by Eqs. (2) and (3).

$$S_i = \frac{A_{ci}}{A_{si}} \times 100\% \quad (2)$$

$$\bar{S} = \frac{1}{k} \sum_{i=1}^k \frac{A_{ci}}{A_{si}} \times 100\% \quad (3)$$

where k is the total number of CT scanning images; A_{ci} is the pixel area of the cracks in the i^{th} CT scanning image; A_{si} is the total pixel area in the i^{th} CT scanning image.

Since the scanning interval was small enough, 85 CT scanning images were selected at equal intervals to calculate the surface crack ratio, and the surface crack ratio distributed along the height of the sample was obtained. Figure 6 shows the variation curves of the surface crack ratio and sample height. With the decrease in water content, the average surface crack ratio increased from 3.75% to 9.82%. At the same time, the variation trend of the surface crack ratio along the sample height also showed a certain regularity. When the water content was 24.0%, the surface crack ratio of expansive soil distributed along the sample height fluctuated from 2.33% to 6.03%, and the difference between the peaks was 3.70%. When the water content was 20.1%, the surface crack ratio fluctuated between 2.83% and 8.73%, and the difference between the peaks was 5.90%. When the water content was reduced to 15.8%, the maximum surface crack ratio reached 13.94%, and the minimum surface crack ratio was only 5.51%. At this time, the difference between the two was 8.43%, indicating that the crack distribution became more uneven.

3.3 Three-dimensional cracks

The reconstructed 3D digital model of expansive soil is presented in Fig.7. One can see from Fig.7(a), at the initial water content, the surface of the expansive soil sample was smooth and there was no obvious surface defect. As shown in Fig.7(b), when the water content decreased from 24.0% to 20.1%, depression and shrinkage occurred locally in the expanded soil sample, and small cracks began to appear on the surface of the soil sample. As the water content decreased to 15.8%, the shrinkage of the soil sample gradually intensified, and the fine cracks propagated into the connected oblique cracks. Several interleaved long cracks on the surface of the three-dimensional

soil model could be observed in Fig.7(c). In Fig.7(d), when the water content dropped to 12.0%, the extreme desiccation effect made the surface cracks run through

the whole soil sample from top to bottom, and the uneven deformation and volumetric shrinkage of the surface of the soil sample were further aggravated.

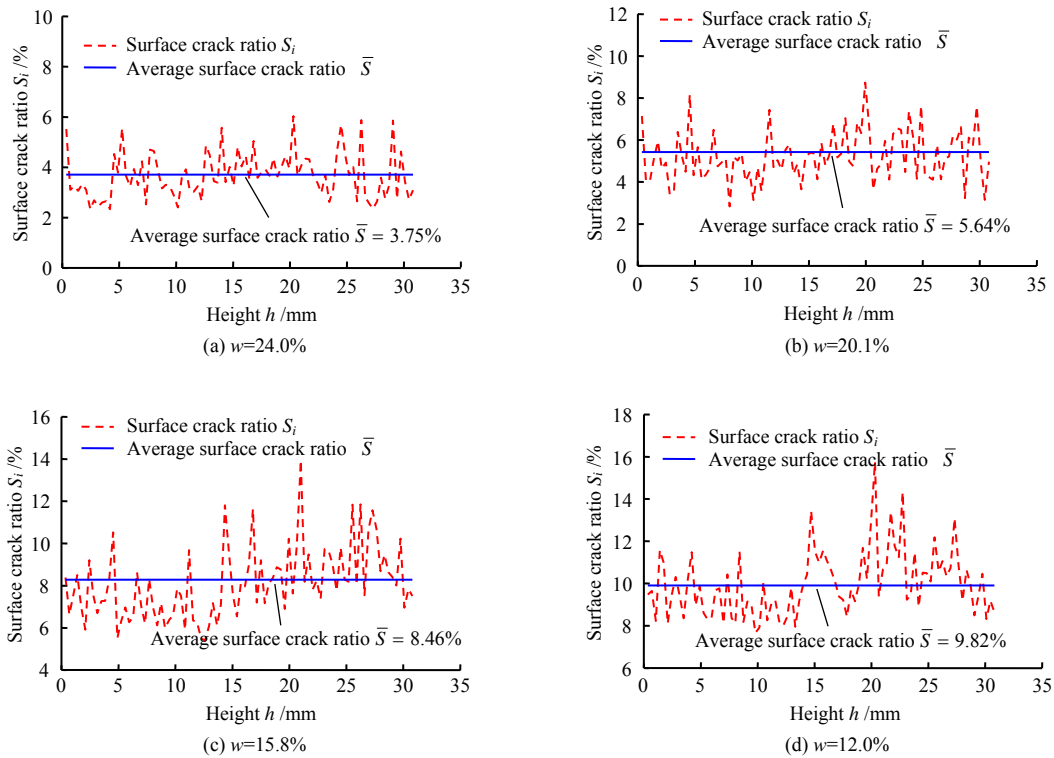


Fig. 6 Variation of surface crack ratio at different sample heights

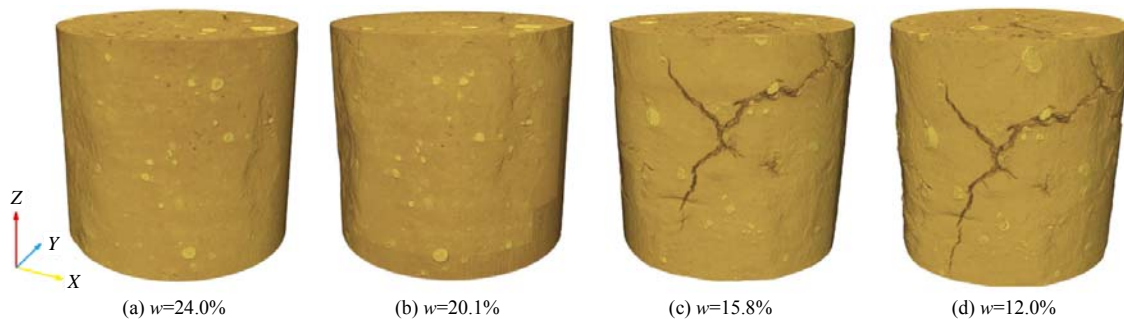


Fig. 7 3D reconstruction model of expansive soil sample

To display the spatial evolution characteristics of the desiccation crack in expansive soil, a 3D digital model of the cracks was obtained by using the 3D reconstruction technique. The volume, size, and geometric shape parameters of all the cracks were calculated by the number and distribution of spatial pixels. Considering that the resolution of micro-CT scanning technology was difficult to identify the tiny pores between clay particles, the volume of the crack obtained in the test was greater than 0.001 mm^3 . According to the volume and geometric characteristics of cracks, cracks with a volume greater than 0.1 mm^3 and an aspect ratio greater than 3 were defined as connected cracks, otherwise, they were named independent cracks. Figure 8 presents the 3D digital models of the cracks in expansive soil. Figure 8 (a) shows the overall occurrence morphology of cracks, in which the

connected cracks mainly existed in strip geometry while the independent cracks were mostly irregular spheroid geometry. It can be observed from Fig. 8 (b) that during the drying process, the number of independent cracks in the expansive soil sample decreased slightly. As shown in Fig.8 (c), at the initial water content ($w = 24.0\%$), there were relatively few connected cracks inside the expansive soil sample, which were mainly distributed in the local area of the soil sample. With the water content drying to 20.1%, the volume of connected cracks increased. When the water content reached 15.8%, the connected cracks in expansive soil were interconnected, forming a complex crack network. When the water content decreased to 12.0%, the connected cracks further coalesced, and the crack network almost covered the entire internal space of the expansive soil sample.

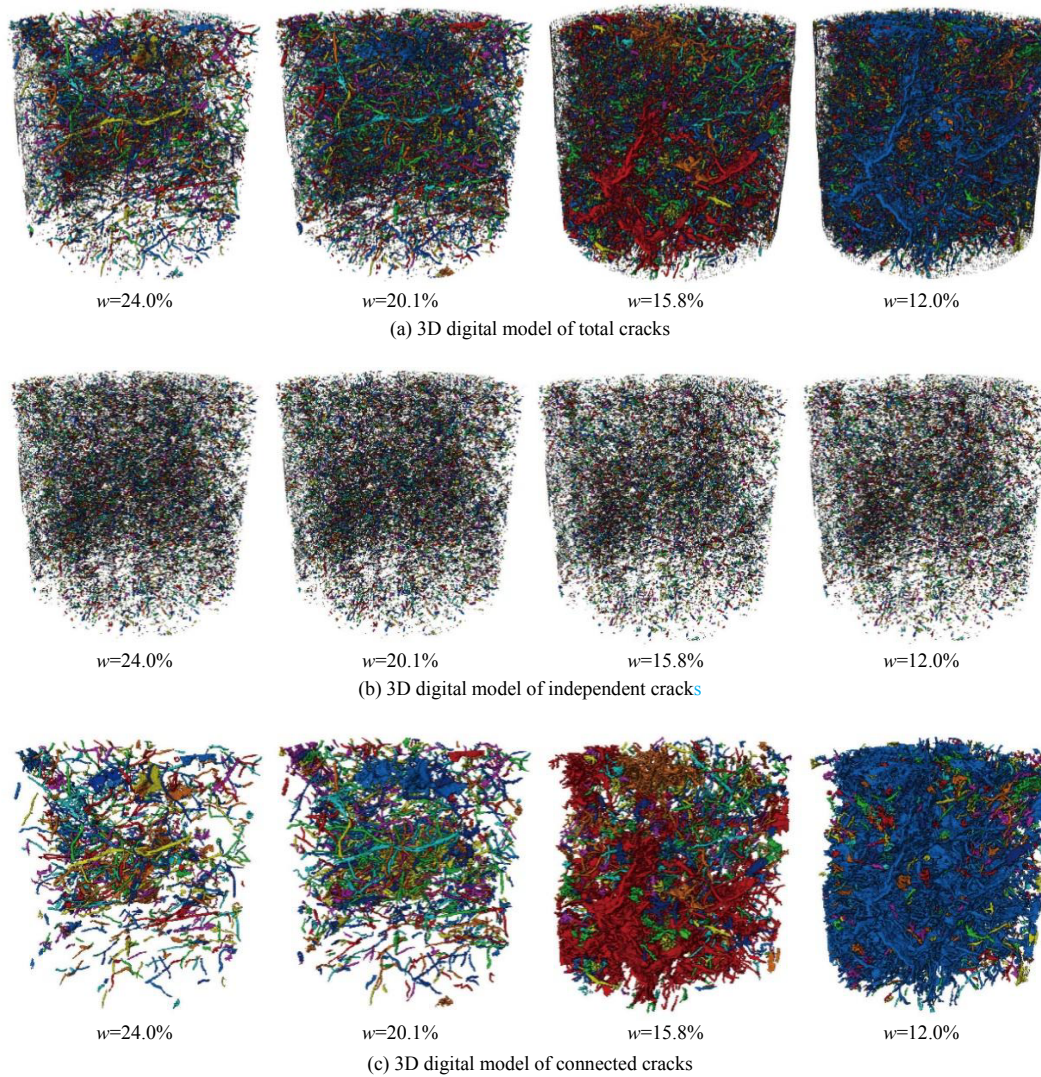


Fig. 8 3D digital model of the cracks in expansive soil

To quantitatively study the evolution law of cracks in expansive soil, the volume of independent cracks, connected cracks and total cracks were statistically analyzed according to the statistical results of the 3D digital model. According to Eqs. (4)–(6), the independent crack ratio ϕ_d , connected crack ratio ϕ_c , and total crack ratio ϕ of the expansive soil samples under different water contents were computed, as shown in Fig. 9.

$$\phi_d = \frac{\sum_i^n v_{dpi}}{V_{tot}} \times 100\% \quad (4)$$

$$\phi_c = \frac{\sum_i^m v_{cpi}}{V_{tot}} \times 100\% \quad (5)$$

$$\phi = \phi_d + \phi_c \quad (6)$$

where n and m are the number of independent cracks and connected cracks, respectively; v_{dpi} and v_{cpi} are the pixel volumes of the i^{th} independent crack and the i^{th} connected crack, respectively; and V_{tot} is the total pixel volume of the soil sample.

Figure 9 shows that the total crack ratio and connected crack ratio present an overall upward trend with the decrease in water content. At the initial drying stage, the surface defects of the expanded soil sample were small, and the water evaporation was slow. The increase in total crack ratio and the connected crack ratio was relatively small, 1.89% and 2.03%, respectively. When the water content decreased from 20.1% to 15.8%, several deep cracks extended into the soil sample and appeared on the surface of the expansive soil sample. In this case, the cracks developed rapidly due to intensified water evaporation. At the same time, the total crack ratio and the connected crack ratio increased significantly, reaching 2.82% and 2.30%, respectively. In the process of water content decreasing from 15.8% to 12.0%, the increment of total crack ratio and connected crack ratio gradually decreased to 1.36% and 1.92%, respectively. This is because when the water content approached the shrinkage limit, the shrinkage deformation tended to be stable. The overall fluctuation of the independent crack ratio during drying was small, and the overall variation was only 0.18%. This is mainly due to the continuous emergence

of new independent cracks during the process of decreasing water content in the expansive soil sample, meanwhile independent cracks propagating and coalescing to form connected cracks.

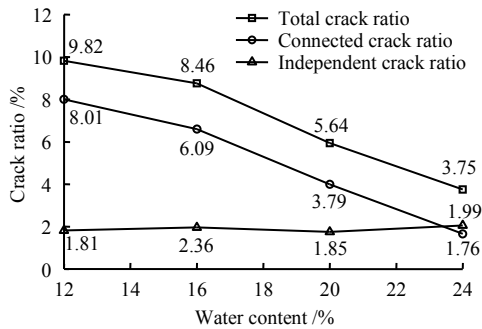


Fig. 9 Variation curves of volumetric crack ratio under different water contents

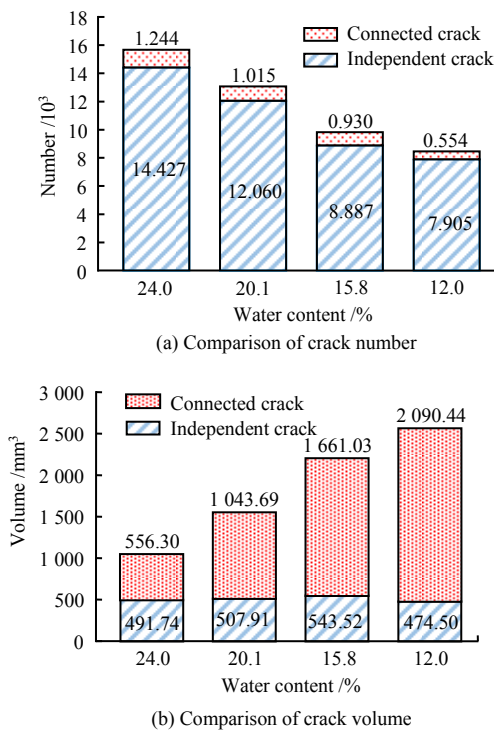


Fig. 10 Comparison of crack number and crack volume under different water contents

In order to further clarify the evolution characteristics of cracks in expansive soil during the drying process, the number and volume of connected cracks and independent cracks were statistically analyzed, and the results are illustrated in Fig.10. With the decrease in water content, the number of both connected cracks and independent cracks decreased. The volume of connected cracks increased significantly, but the volume of independent cracks increased first and then decreased. In the process of water content decreasing from 24.0% to 12.0%, the number of connected cracks decreased by 55.57% and the number of independent cracks decreased by 45.21%. The volume of connected cracks increased from 556.30 mm³ to 2 090.44 mm³, increasing by 1 534.14 mm³, while the volume of independent cracks decreased by 3.51%. The statistical results show

that although the number of connected cracks in expansive soil only accounted for 6.55%–9.47% of the total number of cracks, the volume of connected cracks exceeded more than 53.08% of the volume of total cracks. In addition, during the drying process, the volume proportion of connected cracks continued to increase and finally reached 81.50%, indicating that the connected crack was the key factor determining the overall development of internal cracks in expansive soil.

3.4 Pore network model

For the three-dimensional crack model, the ‘ball-and-stick model’ was used to simulate the pore network [22–24], and then the dimension and connectivity characteristics of the cracks were analyzed. The ‘ball-and-stick model’ refers to arbitrarily selecting a point in the pore voxel and taking this point as the center of the ball to extend around to the edge skeleton voxel. All the contained voxels are called the largest ball. The ‘pore’ and ‘throat’ in the pore network model are determined by finding the minimum ball between the local maximum ball and multiple maximum balls, which correspond to the spheroid independent crack and the long strip connected crack inside the expansive soil sample. Therefore, the crack structure in expansive soil can be equivalent to a network model composed of balls and sticks, namely, the pore network model. A cube with a size of 20 mm was extracted from the interior of the expansive soil sample as the pore network model, as shown in Fig. 11.

In the pore network model, the idealized ball represents the pore, and the radius of the ball is the equivalent pore radius. The relatively narrow pore channel connecting the pores is the pore throat, which is represented by the stick in the model. The size of the throat is often measured by the radius of the largest ball through which it can pass, known as the throat radius. The distance between two adjacent pores is expressed by the length of the throat. The coordination number of pore throat refers to the number of throats connected by a single pore, and it is an important parameter to describe the connectivity between pores. Its average value represents the average pore throat coordination number of the structure. The larger the coordination number represents the better the connectivity of the structure.

The parameters of the extracted 3D pore network model were calculated, and the dimension parameters, including equivalent pore radius, throat radius, throat length and coordination number were obtained. The crack structure of expansive soil was quantitatively characterized according to the calculated pore network model parameters.

Based on the results in Table 2, with the decrease in water content, the pore network model parameters of expansive soil, namely, equivalent pore diameter, throat radius, throat length, and coordination number had an increasing trend. The pore size ranged from 107 to 123 μm and increased continuously during the drying process. The radius and length of the pore throat were distributed in the range of 42–56 μm and

364–409 μm and showed an increasing trend with the decrease of water content on the whole, but there were small fluctuations in the local range. When the water content varied in the range of 20.1% to 15.8%, the radius and length of the pore throat slightly decreased, which was due to a large number of tiny throats produced during drying. In addition, the calculation results also showed that with the decrease in water content, the average coordination number of the expansive soil samples gradually increased, indicating that the connectivity of the mesocracks was continuously enhanced in the process of desiccation.

3.5 Variation characteristics of the mesostructure

To demonstrate the evolution characteristics of the mesostructure of expansive soil, the expansive soil samples before and after drying were analyzed by scanning electron microscope (SEM). The mesostructure morphology of soil samples with a magnification of 500 times was obtained, as shown in Fig.12. One can

see from Fig. 12(a), at the natural water content, the clay minerals of expansive soil were in a laminated structure, and multiple pieces of clay minerals stacked into aggregates. The mesostructure was closely arranged, and no obvious macropores were observed between clay particles. In Fig.12(b), after drying, the boundary between clay particles and pores inside the expansive soil sample was clear, and the flaky clay particles at the edge of the pores had face-to-edge contact. The change of SEM images showed that the mesostructure of expansive soil had changed significantly before and after drying. The density of soil samples decreased and the development of interparticle pores increased greatly. Therefore, the connectivity of mesocracks in expansive soil was significantly related to the arrangement of clay particles and the development of interparticle pores. In addition, the SEM results also verified the validity and accuracy of the micro-CT scanning results.

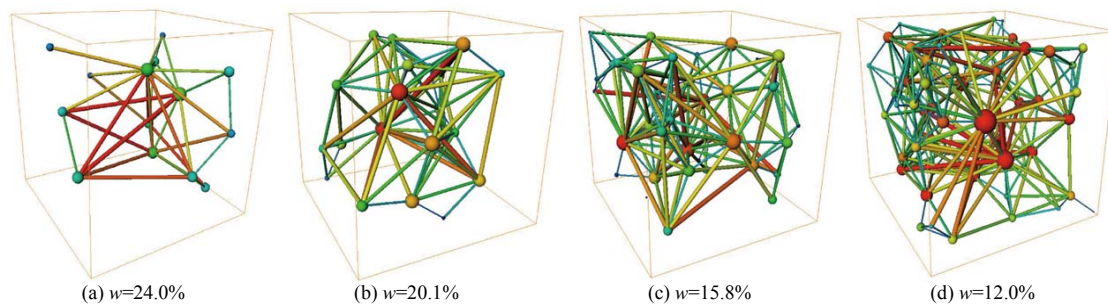
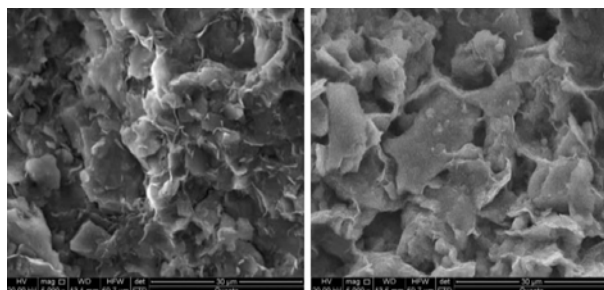


Fig. 11 Schematic diagram of pore network model under different water contents

Table 2 Calculation parameters of pore network model

Water content /%	Mean pore radius / μm	Mean pore throat radius / μm	Mean pore throat length / μm	Mean pore-throat coordination number
24.0	107.23	42.64	364.13	3.40
20.1	114.18	45.35	388.26	4.62
15.8	118.24	45.06	388.10	5.67
12.0	122.61	55.92	408.09	6.21



(a) Before drying ($w=24.0\%$) (b) After drying ($w=12.0\%$)

Fig. 12 SEM images of expansive soil during drying

4 Conclusions

(1) The 3D reconstructed model obtained by micro-CT scanning technology can well reflect the volumetric shrinkage characteristics of the expansive soil sample in the process of desiccation, and the calculated results of the volume of the scanned area are close to the

measured results. With the decrease in water content, the volume of the soil sample decreases first rapidly and then slowly. After the drying test, the volume of the expansive soil sample is reduced by 1.83 cm^3 , and the volumetric shrinkage rate is about 6.54%.

(2) With the decrease in water content, the average surface crack ratio of the expansive soil sample increases continuously. The uneven degree of crack distribution increases at the initial stage and exhibits a stable trend subsequently. Based on the dimension and geometric characteristics of cracks, the mesocracks in expansive soil can be divided into connected cracks and independent cracks. In the process of desiccation, both the total crack ratio and the connected crack ratio show an increasing trend, but the growth rate significantly decreases when the water content is lower than 15.8%, and the variation of independent cracks is small.

(3) In the process of desiccation, the number of connected cracks in expansive soil only accounts for 6.55%–9.47% of the total number of cracks, but the volume of connected cracks reaches 53.08%–81.50% of the total crack volume, indicating that connected cracks are the key factor determining the development of cracks in expansive soil.

(4) The ‘ball-and-stick model’ can effectively simulate the spatial distribution characteristics of cracks in the expansive soil sample. In the process of

desiccation, the parameters for pore network model of expansive soil, namely, average pore radius, throat radius, throat length, and pore throat coordination number, have an increasing trend. The coordination number represents the internal connectivity of the soil sample, indicating that the connectivity of cracks in the expansive soil samples is gradually enhanced during drying.

(5) The clay minerals in the undisturbed expansive soil are closely arranged in a laminated structure. Under the effect of desiccation, the pores between soil particles are significantly expanded, and the evolution of the micro-pore structure has an important effect on the formation and connection of shrinkage mesocracks.

References

- [1] IPCC. Climate change 2021: the physical science basis[M]. Cambridge: Cambridge University Press, 2021.
- [2] MEHTA B, SACHAN A. Effect of mineralogical properties of expansive soil on its mechanical behavior[J]. *Geotechnical and Geological Engineering*, 2017, 35(6): 2923–2934.
- [3] SHI B, JIANG H T, LIU Z, et al. Engineering geological characteristics of expansive soils in China[J]. *Engineering Geology*, 2002, 67(12): 63–71.
- [4] KONG Ling-wei, LI Xiong-wei, GUO Ai-guo, et al. Preliminary study on engineering behaviors and water retention characteristics of expansive soil under influence of drying rate[J]. *Chinese Journal of Geotechnical Engineering*, 2009, 31(3): 335–340.
- [5] CAI Zheng-yin, ZHU Xun, HUANG Ying-hao, et al. Influences of freeze-thaw process on evolution characteristics of fissures in expansive soils[J]. *Rock and Soil Mechanics*, 2019, 40(12): 4555–4563.
- [6] LUO Zhao-gang, WANG Shi-ji, YANG Zhen-bei. Quantitative analysis of fracture evolution of expansive soils under wetting-drying cycles[J]. *Rock and Soil Mechanics*, 2020, 41(7): 2313–2323.
- [7] KONG Ling-wei, CHEN Jian-bin, GUO Ai-guo, et al. Field response tests on expansive soil slopes under atmosphere[J]. *Chinese Journal of Geotechnical Engineering*, 2007, 29(7): 1065–1073.
- [8] YANG He-ping, ZHAN Wen-tao, XIAO Jie, et al. Soil property testing of Nanning expansive soil as embankment filler[J]. *China Journal of Highway and Transport*, 2011, 24(1): 1–7, 19.
- [9] YAO Hai-lin, ZHENG Shao-he, CHEN Shou-yi. Analysis on the slope stability of expansive soils considering cracks and infiltration of rain[J]. *Chinese Journal of Geotechnical Engineering*, 2001, 23(5): 606–609.
- [10] AN R, KONG L W, LI C S. Pore distribution characteristics of thawed residual soils in artificial frozen-wall using NMRI and MIP measurements[J]. *Applied Sciences*, 2020, 10(2): 544.
- [11] HU Dong-xu, LI Xian, ZHOU Chao-yun, et al. Quantitative analysis of swelling and shrinkage cracks in expansive soil[J]. *Rock and Soil Mechanics*, 2018, 39(Suppl.1): 318–324.
- [12] AN Ran, KONG Ling-wei, LI Cheng-sheng, et al. Strength attenuation and microstructure damage of granite residual soils under hot and rainy weather[J]. *Chinese Journal of Rock Mechanics and Engineering*, 2020, 39(9): 1902–1911.
- [13] CHEN Liang, LU Liang. Investigation on the characteristics of volumetric change during the wet-dry cycle of the soil[J]. *Chinese Journal of Underground Space and Engineering*, 2013, 9(2): 229–235.
- [14] SHI B X, CHEN S S, HAN H Q, et al. Expansive soil crack depth under cumulative damage[J]. *The Scientific World Journal*, 2014, 2014: 498437.
- [15] TANG Chao-sheng, CUI Yu-jun, TANG Anh-minh, et al. Shrinkage and desiccation cracking process of expansive soil and its temperature-dependent behaviour[J]. *Chinese Journal of Geotechnical Engineering*, 2012, 34(12): 2181–2187.
- [16] TANG Chao-sheng, SHI Bin, LIU Chun. Study on desiccation cracking behaviour of expansive soil[J]. *Journal of Engineering Geology*, 2012, 20(5): 663–673.
- [17] LU Zai-hua, CHEN Zheng-han, PU Yi-bin. A CT study on the crack evolution of expansive soil during drying and wetting cycles[J]. *Rock and Soil Mechanics*, 2002, 23(4): 417–422.
- [18] Ministry of Water Resources of the People's Republic of China. GB/T 50123—2019 Standard for geotechnical testing method[S]. Beijing: China Planning Press, 2019.
- [19] WANG G, SHEN J N, LIU S M, et al. Three-dimensional modeling and analysis of macro-pore structure of coal using combined X-ray CT imaging and fractal theory[J]. *International Journal of Rock Mechanics and Mining Sciences*, 2019, 123: 104082.
- [20] BRAZ D, BARROSO R C, LOPES R T, et al. Evaluation of scatter-to-primary ratio in soil CT-imaging[J]. *Radiation Physics and Chemistry*, 2001, 61(3-6): 747–751.
- [21] VAN STAPPEN J F, DE KOCK T, DE SCHUTTER G, et al. Uniaxial compressive strength measurements of limestone plugs and cores: a size comparison and X-ray CT study[J]. *Bulletin of Engineering Geology and the Environment*, 2019, 78(7): 5301–5310.
- [22] DONG H, BLUNT M J. Pore-network extraction from micro-computerized-tomography images[J]. *Physical Review E*, 2009, 80(3): 036307.
- [23] DU Y J, JIANG N J, LIU S Y, et al. Engineering properties and microstructural characteristics of cement-stabilized zinc-contaminated kaolin clay[J]. *Canadian Geotechnical Journal*, 2014, 51(3): 289–302.
- [24] WU Y Q, TAHMASEBI P, LIN C Y, et al. Effects of micropores on geometric, topological and transport properties of pore systems for low-permeability porous media[J]. *Journal of Hydrology*, 2019, 575: 327–342.